Applied Energy 372 (2024) 123732

Contents lists available at ScienceDirect

Applied Energy

journal homepage: www.elsevier.com/locate/apenergy

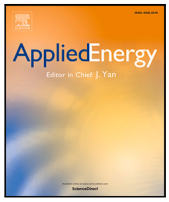

Optimal sizing of battery energy storage system for local multi-energy systems: The impact of the thermal vector

Philipp Glücker [a,b,c,*], Thiemo Pesch [a], Andrea Benigni [a,b,d]

[a] Forschungszentrum Jülich GmbH, Institute of Climate and Energy Systems, ICE-1: Energy Systems Engineering, Jülich 52425, Germany
[b] RWTH Aachen University, Aachen 52056, Germany
[c] Department of Electrical and Electronic Engineering, The University of Melbourne, Melbourne, Victoria 3010, Australia
[d] JARA-Energy, Jülich 52425, Germany

ARTICLE INFO

Keywords:
Battery energy storage system
Community battery
Integrated optimisation
Local energy community
Multi-energy system

ABSTRACT

Battery energy storage systems (BESS) can complement the variability of local renewable energy sources. However, existing research focuses on the design of BESS for electricity systems, mainly neglecting interaction with other energy vectors, e.g., the thermal vector. This study investigates the impact of explicitly modelling the thermal vector on the optimal design of BESS within local multi-energy systems. A holistic problem, including the nonlinear representation of the AC power flow, was developed within a non-convex mixed integer quadratically constrained program formulation. Two modelling approaches were employed: the explicit modelling of the thermal vector, and its implicit consideration within an *all-electric* demand model. These approaches were applied to investigate the impact of neglecting the thermal vector on the optimal BESS design in two real-world case studies. A constant and a time-varying electricity tariff, and three different solar irradiance scenarios were investigated. The results show significant BESS oversizing, higher annual costs and higher global warming impact when neglecting the explicit model of the thermal vector, both within a building and a local energy community. A time-varying electricity tariff enhances the BESS oversizing, with up to 20.5% oversizing for the BESS for a high solar irradiance scenario. Moreover, the annual costs of the *all-electric* demand model are around 8% higher compared to the explicit multi-energy model. Our findings clearly state the importance of explicitly modelling the coupled thermal vector during the sizing of electrical storage systems.

1. Introduction

The goal of limiting the global temperature rise to 1.5 °C requires a rapid transition towards low-carbon technologies and different energy system designs [1]. An emerging concept for future energy systems are local energy communities (LEC), i.e., organisations or groups of individuals that jointly generate, distribute and consume energy within a specific geographic area. Local energy communities are recognised by the European Union in the EU Clean Energy Package as future key features to involve individual households and value-driven organisations, rather than profit-driven companies [2]. The interest in LECs is driven by several factors, including a way to increase the share of renewable energy in the grid, create a more decentralised energy system and promote energy efficiency by avoiding transmission losses over long distances [3–5].

A common way to increase the self-sufficiency of LECs or a building equipped with local renewable energy sources (RES) such as photovoltaic (PV) arrays is the addition of battery electrical storage systems (BESS). Both within single buildings and LECs, BESS can reduce the peak power of the electricity import and export, increase the self-consumption rate of the energy system combined with RES, and reduce annual costs [6–8]. Moreover, a communal BESS within an energy community, such as a LEC, has demonstrated its effectiveness in harnessing the full potential of energy systems, in particular in terms of cost savings, energy storage utilisation and self-sufficiency of the overall energy system [9–11]. However, these studies usually completely neglect or merely include the heating demand within so-called *all-electric* demands only. Representing heating demand as fixed equivalent electrical demand implies no interaction between heat and power vectors. Yet, the shift towards low-carbon technologies incentivises the electrification

* Corresponding author at: Forschungszentrum Jülich GmbH, Institute of Climate and Energy Systems, ICE-1: Energy Systems Engineering, Jülich 52425, Germany.
E-mail addresses: p.gluecker@fz-juelich.de (P. Glücker), t.pesch@fz-juelich.de (T. Pesch), a.benigni@fz-juelich.de (A. Benigni).

https://doi.org/10.1016/j.apenergy.2024.123732
Received 20 December 2023; Received in revised form 14 May 2024; Accepted 13 June 2024
Available online 27 June 2024

Nomenclature

Indices and Set

i, $\mathbb{I}$	Electric bus index, set of electric buses
k, $\mathbb{K}$	Electric bus index, set of electric buses
s, $\mathbb{S}$	Scenario day index, set of scenarios
t, $\mathbb{T}$	Time step index, set of time steps

Parameters

Δt	Time step [h]
$\eta_{\text{bess}}^{\text{in/out}}$	BESS charging / discharging efficiency [%]
$\underline{C}_{\text{bess}}$ / $\overline{C}_{\text{bess}}$	Minimum / maximum BESS capacity [kWh]
$\underline{U}_{\text{i}}$ / $\overline{U}_{\text{i}}$	Lower / upper voltage limit at bus i [p.u.]
a_{ik}	Transformer tap ratio between buses i and k
b_{ik}	Line susceptance between buses i and k [p.u.]
$b_{\text{ik}}^{\text{sh}}$	Shunt susceptance between buses i and k [p.u.]
C_{fix}	Annual fixed cost [€]
c_{fix}	Relative fixed cost [%]
C_{i}	Overall investment cost [€]
C_{tac}	Total annualised cost [€]
C_{var}	Annual variable cost [€]
c_{var}	Variable cost [€/kWh]
f_{ann}	Annuity factor [1/a]
g_{ik}	Line conductance between buses i and k [p.u.]
K_{bd}	Thermal building capacitance [kWh/°C]
$o_{s,t}$	Value of operational quantity [kWh]
w_s	Weight of scenario day d

Variables

$\dot{m}_{\text{hp}}^{\text{eva/con}}$	HP evaporator / condenser mass flow rate [kg/s]
$\dot{m}_{\text{hs}}$	Mass flow rate of heat source [kg/s]
$\dot{m}_{\text{ltdh}}$	Mass flow rate within LTDH network [kg/s]
$\dot{Q}_{\text{hp}}^{\text{out}}$	Thermal output power of heat pump [kW_{th}]
b_{bess}	Binary variable for BESS installation
$b_{\text{hp}}^{\text{op}}$	Binary variable for heat pump operation
C_{bess}	BESS capacity to be installed [kWh]
E_{i}	Real part of complex voltage at bus i [p.u.]
F_{i}	Imaginary part of complex voltage at bus i [p.u.]
$P_{\text{gr}}^{\text{in / out}}$	Active power exchange with external grid [kW]
P_{pump}	Active power of network pump [kW]
Q_{gr}	Reactive power exchange at external grid [kVAr]
T_{bd}	Building temperature [°C]
$T_{\text{ltdh}}^{\text{fl}}$	Flow temperature within LTDH network [K]
$T_{\text{ltdh}}^{\text{ret}}$	Return temperature within LTDH network [K]
U_{i}	Voltage magnitude at bus i [p.u.]
P_{hp}	Active power input of heat pump [kW]
P_{i}	Active power at bus i [kW]
Q_{i}	Reactive power at bus i [kVAr]
SOC_{bess}	BESS state of charge [kWh]
SOC_{tes}	TES state of charge [kWh]

of heating solutions, e.g., replacing gas and oil heating systems with electric heat pumps. The increasing heat pump installations couple the electricity and the heating sector and thus complement the concept of local multi-energy systems (MES), which contain multiple energy commodities, e.g., electricity, heat and gas. By exploiting the interdependencies and interactions of the energy flows and storage options of the different commodities, MES can further increase grid stability and reduce energy costs [12–15]. Therefore, only considering the electrical domain for the design of electrical components – even when considering for instance the electrical consumption due to heating as a predefined time series – neglects possible flexibility provided by the interaction between coupled commodities.

A model-based optimisation is a suitable tool for the operation and planning of energy systems [16]. However, the modelling for the design and operation of MES can be technically challenging. Integrating different technologies with interdependent commodities must consider the coordination of energy flows between different sources and storage options. These complex constraints must already be considered during the design stage of system components, as their design determines the operation of the multi-energy system [17,18]. This results in complex problem formulations, and thus the detailed model representation of multiple commodities for optimisation purposes can be computationally expensive.

Existing work tackles the computational and modelling challenges of the design and operational optimisation of MES by an iterative approach or by using mixed-integer linear programming (MILP) models. An iterative approach lifts the computational burden of modelling an MES. Here, the first stage usually includes the linear operational optimisation of the components without networks. Based on the output of the first stage, the second stage then simulates the nonlinear network operation. Identified power losses and violated network constraints are linearised and included in the next iteration of the linear model until convergence. For instance, the iterative approach is applied for the operational optimisation of MESs with integrated electricity-heat-gas networks [19–22]. However, these studies either model only a linear behaviour of networks and components, or solely focus on the MES operation and neglect the component design.

Using MILP models is a common way of modelling the design and operation of distributed MES by one holistic problem formulation [23,24]. Here, the nonlinear behaviour of energy components such as the power grid and heating network is linearised. The linearisation is applied for the consideration of seasonal storage [25,26], in large-scale transmission and investment planning systems [27,28], and the representation of an MES as an energy hub, which models the conversions of different energy forms as a multi-input multi-output conversion component [29]. For instance, an optimal capacity design and operation of islanded energy hubs supporting electricity and heat demand is investigated in [30]. A chance-constrained optimisation and a robust counterpart problem formulation are employed to address stochastic RES generation and load while balancing robustness and cost efficiency. The energy system consists of the energy vectors electricity, gas, hydrogen and heat, while the gas and electrical networks were explicitly modelled. The latter is modelled by the linear DC power flow, which is an accurate approximation for high-voltage networks, but does not apply to medium- and low-voltage networks. Another work [31] presents a MILP formulation combined with energy hubs for integrated design and operation of distributed energy systems and optimal heating network layouts. While their approach provides valuable insights into the design and operation of energy hubs, it overlooks BESS sizing considerations and linearises the physical behaviour of components and networks. Neglecting nonlinear behaviour or losses in the power grid could lead to suboptimal design choices. In another work by [32], the optimal design and operation of PV-battery systems considering coupled HPs are analysed. Their MILP model demonstrates the impact of increased HP penetration on the return of PV-battery systems. However, this study does not consider an electrical network or heating network In [33], a generic framework was developed for the optimal design and operation of distributed energy systems. While their multi-objective optimisation with an augmented epsilon-constrained technique accounts for cost and global warming impact greenhouse gas emissions, it is based on a MILP formulation which neglects nonlinear component and network behaviour. Similarly, a framework for designing sustainable multi-vector energy hubs supplying electricity and thermal energy

was proposed in [34], where detailed technology models are used to optimise the energy system regarding global costs and emissions via a multi-objective function. However, a MILP formulation is used and no internal power grid is considered.

While the issue of designing and operating a multi-vector energy hub is widely investigated in the scientific literature, the consideration of detailed component and network models is not yet fully explored for these studies. With the increasing electrification of the heating sector and its coupling with the electricity sector, a comprehensive analysis involving detailed modelling of all coupled sectors becomes crucial for optimal design choices. In particular, despite the above-displayed advantages of BESS for energy communities, there is a lack of studies that thoroughly analyse the sizing of BESS within a MES. More specifically, there is a gap in understanding how incorporating the coupled heat vector influences the design of BESS: how the thermal inertia of a building affects the BESS sizing. The impact of considering heat on the sizing of BESS has, to the best knowledge of the authors, not been assessed in the literature. Moreover, the design and operation of MES within one holistic optimisation problem considering the heating network and exact power flow equations have not been presented yet in the literature.

The presented work bridges the above-mentioned knowledge gaps. A BESS is to be retrofitted for an existing MES with coupled electricity and heat, which is assumed to be controlled by a perfect energy management system. The key novelty and contributions of the work presented in this paper are as follows:

- Definition of an MES model with heat and electricity vectors for the optimisation-based sizing of a BESS, including the nonlinear representation of the AC power grid, the heating network and a quadratic heat pump model
- Comparison between a integrated multi-energy system and an *all-electric* system for the optimal sizing of a BESS
- Analysis of different solar irradiance years and time-varying and constant electricity tariffs on BESS sizing
- Application of the multi-energy and *all-electric* modelling approach to two real-world case studies based in Germany (a single building and a local energy community)

The paper is structured as follows. Section 2 introduces the methodology and component modelling of the MES. To investigate the questions mentioned above, two case studies are presented. The results of these studies, including the component design and the system operation, are provided and analysed in Section 4, followed by the discussion of the results. Section 5 concludes the work.

2. Methodology

The flowchart of the implemented algorithms is depicted in Fig. 1. Initially, the input data is pre-processed and clustered into several representative scenario days. Then, these clusters and further parameter data are given to the two-stage stochastic model structure. The first stage determines the optimal investment decisions based on the given set of scenarios for time-varying load profiles, solar irradiation and electricity prices, while the second stage finds the optimal operation strategy of the overall system.

2.1. Component modelling

The modelling approach within this work is based on component-oriented modelling, allowing for a modular and scalable system design and operation which is required for energy communities. In the following, the energy components included in the MES under consideration are introduced and their functionalities are briefly presented. This includes the battery electric storage system, the photovoltaic array, the power grid, the heating network, the heat pump and the thermal building model.

2.1.1. Battery energy storage system

The BESS is modelled as a lithium-ion battery connected to a bidirectional inverter which enables charging and discharging of both active and reactive power. The model includes energy losses considering distinct charging and discharging efficiencies, a self-discharge rate of the battery, and limits on the apparent power, leading to the following governing equations:

$$\frac{\mathrm{dSOC_{bess}}}{\mathrm{d}t} = \frac{\eta^{\mathrm{in}}_{\mathrm{bess}} P^{\mathrm{in}}_{\mathrm{bess}} - P^{\mathrm{out}}_{\mathrm{bess}} / \eta^{\mathrm{out}}_{\mathrm{bess}} - \frac{1}{\tau_{\mathrm{bess}}} \mathrm{SOC_{bess}}}{C^{\mathrm{des}}_{\mathrm{bess}}}, \tag{1}$$

$$S^2_{\mathrm{bess}} = P^2_{\mathrm{bess}} + Q^2_{\mathrm{bess}} \leq \overline{S}^2_{\mathrm{bess}}, \tag{2}$$

$$\underline{P}_{\mathrm{bess}} \leq P_{\mathrm{bess}} \leq \overline{P}_{\mathrm{bess}}, \tag{3}$$

$$\underline{Q}_{\mathrm{bess}} \leq Q_{\mathrm{bess}} \leq \overline{Q}_{\mathrm{bess}}, \tag{4}$$

$$b_{\mathrm{bess}} \underline{C}_{\mathrm{bess}} \leq C^{\mathrm{des}}_{\mathrm{bess}} \leq b_{\mathrm{bess}} \overline{C}_{\mathrm{bess}}, \tag{5}$$

$$P^{\mathrm{in}}_{\mathrm{bess}} \cdot P^{\mathrm{out}}_{\mathrm{bess}} \leq 0. \tag{6}$$

Here, $\mathrm{SOC_{bess}}$ represents the state of charge of the BESS at a specific point in time, $\eta^{\mathrm{in}}_{\mathrm{bess}}$ and $\eta^{\mathrm{out}}_{\mathrm{bess}}$ are the constant charging and discharging efficiencies, $P^{\mathrm{in}}_{\mathrm{bess}}$ and $P^{\mathrm{out}}_{\mathrm{bess}}$ represent the charging and discharging power, and τ_{bess} is the time constant describing the relative self-discharge of the BESS per hour. An upper and lower power limit constrains the charge/discharge power P_{bess}. The upper limit $\overline{P}_{\mathrm{bess}}$ is chosen to be the power to charge/discharge the BESS within one hour, and the lower limit $\underline{P}_{\mathrm{bess}}$ is zero. The BESS capacity $C^{\mathrm{des}}_{\mathrm{bess}}$ is implemented as a design variable which is constrained by a minimum size $\underline{C}_{\mathrm{bess}}$, a maximum size $\overline{C}_{\mathrm{bess}}$, and the binary variable b_{bess} modelling whether the BESS is built. $\underline{C}_{\mathrm{bess}}$ is 5 kWh which is also included in the BESS investment cost (see Eq. (27)), whereas there is no upper limit for the BESS capacity. Furthermore, the incoming or outgoing active power is limited by the power rating $\overline{S}_{\mathrm{bess}}$ of the inverter connected to the BESS, which is equal to the upper power limit of the BESS. Eq. (2) inherently implies that the power inverter can provide positive or negative reactive power within its power limits.

2.1.2. Photovoltaic array

The PV array is implemented as an active power source connected to a DC-AC inverter. The power inverter connected to the PV array can absorb or produce reactive power within a range of the power factor $\cos\varphi \in [0.9_{\mathrm{cap}}, 0.9_{\mathrm{ind}}]$, which is defined as the ratio of active power to apparent power. This leads to the following constraints:

$$-0.484\ P_{\mathrm{pv}} \leq Q_{\mathrm{pv}} \leq 0.484\ P_{\mathrm{pv}}, \tag{7}$$

$$P_{\mathrm{pv}} \leq \overline{P}_{\mathrm{pv}}. \tag{8}$$

Here, Q_{pv} is the reactive power, P_{pv} is the active power supply and $\overline{P}_{\mathrm{pv}}$ represents the maximum power supply of the PV panel determined by the solar irradiance at each time step. Negative reactive power values represent injection and positive values represent consumption of inductive reactive power.

2.1.3. Power grid

The power flow equations are implemented in rectangular coordinates, i.e., an exact representation of the power flow formulation. The nonlinear trigonometric terms of the polar voltage representation as presented in [35] are replaced with bilinear constraints. The non-convex quadratic formulation based on [36] is implemented as follows:

$$U_{\mathrm{i}} = E_{\mathrm{i}} + jF_{\mathrm{i}}, \tag{9}$$

$$P_{\mathrm{ik}} = g_{\mathrm{ik}} a^2_{\mathrm{ik}} \left(E^2_{\mathrm{i}} + F^2_{\mathrm{i}}\right) - g_{\mathrm{ik}} a_{\mathrm{ik}} \left(E_{\mathrm{i}} E_{\mathrm{k}} + F_{\mathrm{i}} F_{\mathrm{k}}\right) - b_{\mathrm{ik}} a_{\mathrm{ik}} \left(F_{\mathrm{i}} E_{\mathrm{k}} - E_{\mathrm{i}} F_{\mathrm{k}}\right), \tag{10}$$

$$Q_{\mathrm{ik}} = -a^2_{\mathrm{ik}} \left(E^2_{\mathrm{i}} + F^2_{\mathrm{i}}\right) \left(b_{\mathrm{ik}} + \frac{b^{\mathrm{sh}}_{\mathrm{ik}}}{2}\right) + b_{\mathrm{ik}} a_{\mathrm{ik}} \left(E_{\mathrm{i}} E_{\mathrm{k}} + F_{\mathrm{i}} F_{\mathrm{k}}\right) - g_{\mathrm{ik}} a_{\mathrm{ik}} \left(F_{\mathrm{i}} E_{\mathrm{k}} - E_{\mathrm{i}} F_{\mathrm{k}}\right). \tag{11}$$

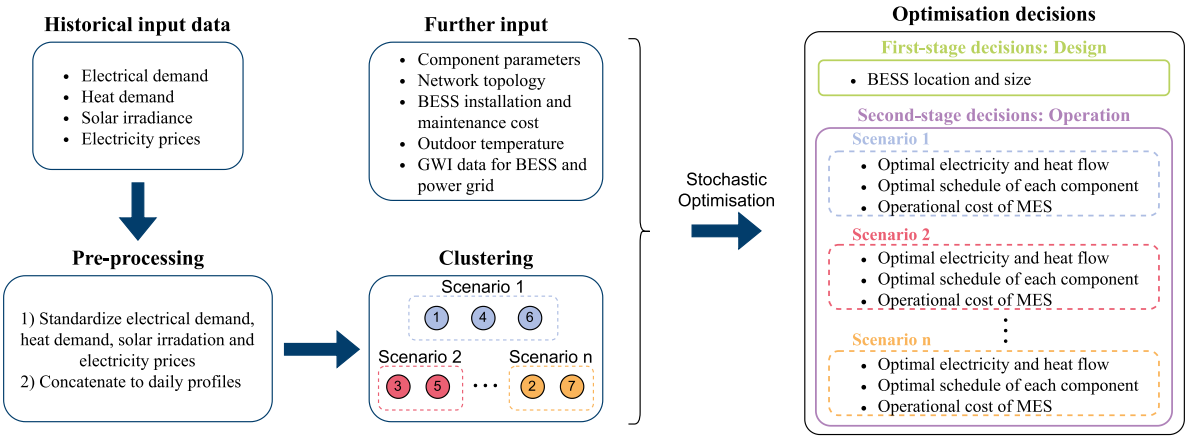

Fig. 1. Flowchart of the implemented algorithm.

Here, E_i represents the real part and F_i the imaginary part of the complex voltage U_i, with $j = \sqrt{-1}$ being the imaginary unit in the complex domain. P_{ik} and Q_{ik} are the active and reactive power transfer across a line from bus i to bus k, b_{ik} is the line susceptance, g_{ik} is the line conductance, b_{ik}^{sh} is the shunt susceptance and a_{ik} is the voltage tap ratio of the transformer with a default value of 1. The magnitude limitations for the voltage rectangular coordinates require functional inequality constraints instead of direct enforcement, as is usually done for the polar coordinates, see [36]. The line capacity limits are included by the following constraints for the bus voltage and the line capacity:

$$(\underline{U}_i)^2 \leq E_i^2 + F_i^2 \leq (\overline{U}_i)^2, \tag{12}$$

$$P_{ik}^2 + Q_{ik}^2 \leq (\overline{S}_{ik})^2. \tag{13}$$

Here, $\underline{U}_i$ and $\overline{U}_i$ represent the lower and upper limit of the voltage magnitude, and $\overline{S}_{ik}$ the apparent power limit of each line.

2.1.4. Heating network

The heating network operates as a low-temperature district heating (LTDH) network. Its lower operating temperature allows for the efficient use of waste heat (WH) as a heat source. This waste heat can come from various sources, e.g., industrial processes or high-performance computers. The LTDH network connects the waste heat with the buildings. To meet the required building supply temperature, heat pumps are employed in each building to elevate the temperature level as needed. The temperature entering the evaporators of the heat pumps is the same for all buildings. The governing equations of the LTDH network are as follows:

$$\dot{m}_{ltdh} = \sum_{bd \in B} \dot{m}_{bd}^{evap}, \tag{14}$$

$$\dot{Q}_{loss} = \left(T_{ltdh}^{fl} - T_{gr}\right) \cdot h_{loss} \cdot A + \left(T_{ltdh}^{ret} - T_{gr}\right) \cdot h_{loss} \cdot A, \tag{15}$$

$$P_{pump} = \frac{\Delta p \cdot \dot{m}_{ltdh}}{\eta_{pump} \cdot \rho_{H_2O}}. \tag{16}$$

Here, T_{ltdh}^{fl} is the flow temperature and m_{ltdh} represents the mass flow of the LTDH network. The heat transfer coefficient is denoted by h_{loss}, A represents the surface area of the pipes and Δp represents the pressure drop of the pipe network. The losses of the network are calculated by a heat loss correlation between the ground temperature, and the respective flow and return temperature of the pipes. The electric power of the pump is denoted as P_{pump}, η_{pump} is the pump efficiency and ρ_{H_2O} is the density of water. Further details on the modelling of the heating network can be found in [37].

2.1.5. Heat pump

The implemented model for the heat pump (HP) is based on a water-to-water heat pump extracting heat from a district heating network at its evaporator side and supplying heat at a higher temperature on its condenser side to the building energy system. The HP is modelled with two ports, one at the evaporator and one at the condenser. Each port is characterised by the flow temperature, the colder return temperature, and the respective mass flow rate. The efficiency of the HP behaves non-linearly, decreasing at lower load conditions due to increased heat transfer rates and increased cycling losses. The detailed model of the heat pump is based on previous work of our research group [37]. The HP model includes the part-load behaviour of the heat pump by a Glover reformulation based on [38,39], which leads to a quadratic formulation of the part-load behaviour. The overall governing equations are as follows:

$$P_{hp} = \dot{Q}_{hp}^{con} - \dot{Q}_{hp}^{eva}, \tag{17}$$

$$\dot{Q}_{hp}^{eva} = \dot{m}_{hp}^{eva} \cdot c_p \cdot \left(T_{hp}^{eva,in} - T_{hp}^{eva,out}\right), \tag{18}$$

$$\dot{Q}_{hp}^{con} = \dot{m}_{hp}^{con} \cdot c_p \cdot \left(T_{hp}^{con,out} - T_{hp}^{con,in}\right), \tag{19}$$

$$P_{hp} \cdot \eta_{hp} \cdot \eta_{hp}^{pl} = \left(\frac{T_{hp}^{con,out} - T_{hp}^{eva,out}}{T_{hp}^{con,out}}\right) \cdot \dot{Q}_{hp}^{con}, \tag{20}$$

$$P_{hp} \cdot T_{hp}^{con,out} \cdot \eta_{hp} = \left(T_{hp}^{con,out} - T_{hp}^{eva,out}\right) \cdot \left(0.029 \cdot \dot{Q}_{hp}^{max} \cdot b_{hp}^{op} + 0.993 \cdot \dot{Q}_{hp}^{con}\right). \tag{21}$$

Here, P_{hp} represents the electric power of the heat pump. $\dot{Q}_{hp}^{con}$ and $\dot{Q}_{hp}^{eva}$ are the thermal power at the condenser and the evaporator with their respective input and output temperatures $T_{hp}^{eva,in/out}$ and $T_{hp}^{con,in/out}$ and their mass flow $\dot{m}_{hp}^{eva/con}$. η_{hp} is the device efficiency of the heat pump and η_{hp}^{pl} represents the part-load efficiency. The device efficiency is assumed to be constant at 0.6. The overall efficiency of the HP is calculated by both the device efficiency and the part-load efficiency, with the latter being integrated into Eq. (21) based on the maximum thermal output power $\dot{Q}_{hp}^{max}$ and a boolean variable b_{hp}^{op} indicating whether the heat pump is operating or not. To reduce the number of quadratic constraints for scalability, a constant temperature difference at the evaporator of $\Delta T = 10\,\mathrm{K}$ is assumed. Additionally, a discontinuous operation of the heat pump is assumed [40], and thus no time-coupling constraints for minimum operational or shutdown times are implemented. The constant parameters in Eq. (21) were fitted to represent the part-load efficiency of water-to-water HPs based on experimental data according to [39].

2.1.6. Thermal building model

In this work, two types of thermal storage systems within a building are considered, namely the hot water storage (HWS) and the dwellings of the building. The HWS stores heated water for domestic use and thus acts as a supply-side buffer, whereas the building dwellings can internally absorb, store and release heat over time and thus help regulate indoor temperature against external temperature fluctuations [41]. The thermal building model combines the HWS and the dwellings of the building within one lumped parameter, which is defined as thermal energy storage (TES). The TES depends on the thermal capacity K_{bd} representing the thermal inertia of the building dwellings and the HWS. The TES is heated up by the thermal power $\dot{Q}_{\mathrm{in}}$ from the HP, and it releases its thermal output power $\dot{Q}_{\mathrm{out}}$ to a deterministic heat demand (HD) which is based on historical data. The temperature T_{bd} represents the building's temperature within its comfort temperature limits, which is assumed to be between 19 °C and 22 °C. The governing equations are as follows:

$$\frac{\mathrm{d}T_{\mathrm{bd}}}{\mathrm{d}t} = \frac{\dot{Q}_{\mathrm{tes}}^{\mathrm{in}} - \dot{Q}_{\mathrm{tes}}^{\mathrm{out}}}{K_{\mathrm{bd}}}, \tag{22}$$

$$\underline{T}_{\mathrm{bd}} \leq T_{\mathrm{bd}} \leq \overline{T}_{\mathrm{bd}}. \tag{23}$$

2.2. Problem formulation and implementation

The case studies are modelled within the open-source energy system optimisation framework COMANDO [42]. Its two-stage stochastic programming structure allows for the optimal design and operation of multi-energy systems such as local energy communities. The system model is composed of the above-described component models. Within a building, the components are connected via balancing nodes, whereas the energy carrier networks of the LEC are represented by the power grid and the heating network components, respectively. This enables the consideration of the interactions between different components, commodities and the overall system, resulting in accurate and comprehensive results.

It is assumed that a centralised instance controls the MES components. In contrast to local control systems that focus on individual components, a centralised coordinated control system considers the optimal operation of the entire MES, including all commodities and their interaction with each other. Such a systematic approach allows the coordinated integration of distributed RES, electrical energy storage systems and the interaction of energy vectors with each other.

The optimisation problem is formulated as a non-convex Mixed-Integer Quadratically Constrained Program (MIQCP). This study aims to determine the most cost-effective battery capacity for a pre-existing MES. This is carried out by minimising the total annualised cost C_{tac} of the MES, calculated as follows:

$$C_{\mathrm{tac}} = C_{\mathrm{i}} f_{\mathrm{ann}} + C_{\mathrm{fix}} + C_{\mathrm{var}}, \tag{24}$$

$$= C_i\, f_{\mathrm{ann}} + c_{\mathrm{fix}}\, C_i + c_{\mathrm{var}} \sum_{s\in\mathbb{S}} w_s \sum_{t\in\mathbb{T}} o_{s,t}\, \Delta\tau. \tag{25}$$

Here, the overall investment cost C_{i}, the annual fixed cost C_{fix} and the variable operating cost C_{var} are considered. $o_{s,t}$ represents the value of an operational quantity with associated cost, e.g., electricity or heat, for a scenario day s and time step t. w_s represents the weight accounting for the number of days assigned to each cluster, Δt represents the chosen time step duration in hours, and f_{ann} is the annuity factor which is calculated as follows:

$$f_{\mathrm{ann}} = \frac{(1+i)^n \cdot i}{(1+i)^n - 1}. \tag{26}$$

Here, a lifetime n of 15 years and an interest rate i of 6% is assumed, resulting in an annuity factor of approximately 0.103 per year.

It is further assumed that the electricity produced by the PV arrays and the heating power supplied by the waste heat are free of charge. The only cost related to the heating supply is the operation of the network pump and the heat pumps, which are included in the power drawn from the external power grid. In the case studies, the variable operational cost depends on the consumed electricity and the respective electricity prices, and thus the operational quantity $o_{s,t}$ refers to the active power drawn from the external grid, which includes the internal power losses of cables and transformers.

In the considered MES, all the components, i.e., PV arrays, heat pumps, thermal energy storage, power grid and heating network, are already installed, except the BESS. Therefore, their investment costs are not included in the optimisation objective, but they only depend on the investment cost for the BESS. The battery design capacity has a minimum size of $\underline{C}_{\mathrm{bess}} = 5\,\mathrm{kWh}$. The battery has a fixed cost of $c_{\mathrm{bess,fix}} = 2.5\%$ of the investment cost per year [43], which covers the annual maintenance cost. The investment cost of the battery is assumed to be linear:

$$C_{\mathrm{I,bess}} = 12000 + 450 \cdot (C_{\mathrm{bess}} - \underline{C}_{\mathrm{bess}}). \tag{27}$$

Here, smaller batteries have a higher cost per installed capacity and bigger batteries have a lower cost per installed capacity.

The expected annual global warming impact (GWI) is further included in our studies as follows:

$$\mathrm{GWI} = \sum_{s\in\mathbb{S}} w_s \sum_{t\in\mathbb{T}} \mathrm{GWI}_{s,t}^{\mathrm{el}}\, \Delta\tau + \mathrm{GWI}^{\mathrm{bess}} \frac{C_{\mathrm{I,bess}}}{n_{\mathrm{bess}}}. \tag{28}$$

Here, $\mathrm{GWI}_{s,t}^{\mathrm{el}}$ is the hourly average GWI of the external power grid and $\mathrm{GWI}^{\mathrm{bess}}$ represents the GWI per capacity of the installed BESS.

3. Case studies

In the following, we introduce the two case studies: the single building and the LEC. Both are modelled as a multi-energy system and as an *all-electric* system, respectively. The *all-electric* system represents the benchmark modelling approach to which the MES model is compared. Finally, the input data for the two case studies is presented.

3.1. Single building

The case study single building is representative of an office building. Two different models are considered for the single building case study, namely the multi-energy building model and the *all-electric* building model as shown in Fig. 2. On the one hand, the multi-energy building model includes the HD and TES and thus accompanies the flexible operation of the heat vector. On the other hand, the *all-electric* building model represents the heat vector solely from an electrical point of view, i.e., the heating demand is included in the load profile of the heat pump, but any operational flexibility of the heating components is neglected. Note that the TES is a lumped parameter representing both the HWS and the thermal inertia of the building dwellings. The difference between the two models is reflected in the change of the active power consumption of the HP being an operational variable for the multi-energy building model, compared to being a parameter determined by the deterministic HD for the *all-electric* building model.

The ED is met by the electricity connection of the building, the BESS, and the PV array. For the multi-energy building, the HD is supplied by the TES which is directly supplied by the heat pump. The building has a connection to the power grid and the heating network. For the *all-electric* building, the heat commodity is disregarded and only the deterministic electricity consumption of the HP is considered, which is directly determined by the HD. Note that the PV panel can consume or inject reactive power, but only generate active power. Within the building, the active power and reactive power are balanced, respectively. Note that this approach can easily be adapted to represent any building and any composition of components within.

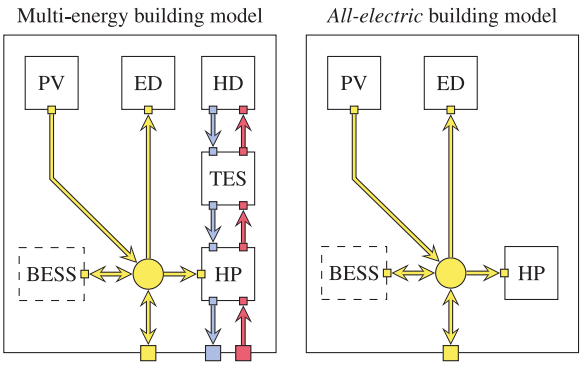

Fig. 2. Internal structure of the multi-energy building model and the *all-electric* building model: photovoltaic (PV) array, electric demand (ED), heat demand (HD), thermal energy storage (TES), heat pump (HP) and the battery energy storage system (BESS) which is to be installed and sized. Electricity is shown in yellow, hot water in red and cold water in blue, with the arrows indicating the energy carrier flow direction.

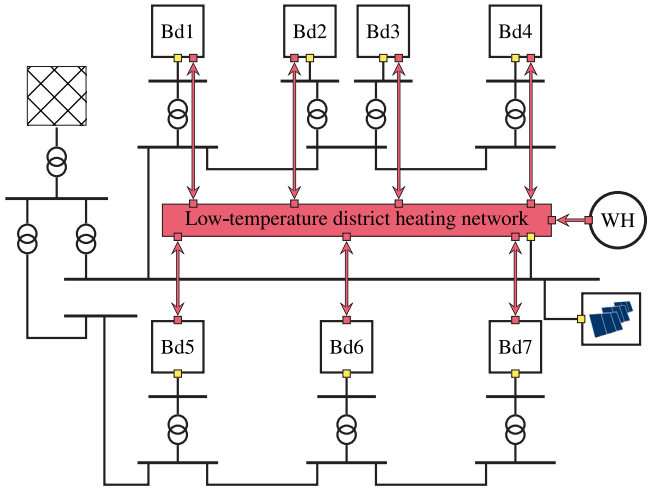

Fig. 3. Local energy community consisting of seven buildings (Bd) including the power grid, the low-temperature district heating (LTDH) network and the waste heat (WH). Note that each building has a rooftop PV array installed.

3.2. Local energy community

The second case study describes a real-world LEC with the commodities electricity and heat, which is part of Forschungszentrum Jülich in Germany. A sketch of the case study including the single-line diagram of the internal power grid and the connections of the heating network is shown in Fig. 3. The LEC is connected to the external power grid at the 110 kV level. The external power is being transformed first to 35 kV and then to 10 kV, where it is connected to two bus bars, each connected to a feeder with several buildings. One community BESS is to be sized and located at the electric bus of one of the seven buildings which represent a mix of office and laboratory buildings. The buildings are connected to the internal power grid at 400 V via transformers, with building two (Bd2) and building three (Bd3) sharing the same electric bus at 10 kV. An additional PV array is directly connected to the upper bus bar.

Similarly to the building case study, this case study is modelled both as a multi-energy LEC model and as an *all-electric* LEC model. Here, the multi-energy building models from the first case study are considered as the buildings in the multi-energy LEC model as depicted in Fig. 2. Each building has a warm water and a cold water connection with the LTDH network, which is supplied by waste heat from a high-performance computer. The evaporator mass flow of the HP along with the warm and cold water flow is connected to the network for each building.

Table 1
Weights of the representative days for the building and the local energy community (LEC).

Building	Day	4	48	174	223	231	319
	Weight	37	69	60	93	64	42
LEC	Day	48	180	231	317	–	–
	Weight	84	152	62	67	–	–

The amount of active and reactive power at each bus bar is determined by the active and reactive power consumption of the connected building, respectively. The active power consumption and generation of the BESS, PV array, ED and HP determine the active power at the bus bar connected to the building. The ED is implemented as a time series. In contrast, the active power input of the HP, the power generation of the PV plant, and the power input and output of the battery are implemented as operational variables, which are determined during the optimisation. The same applies to reactive power. Note that the constant power factor of the electric demand is known beforehand for each time step. In contrast, the reactive power consumption of the heat pump, and the reactive power injection or absorption of the battery and the PV array determine the resulting reactive power at the connected bus bar.

The *all-electric* LEC model only considers electricity and thus represents the heat vector from an electrical point of view, i.e., the seven buildings are modelled as the *all-electric* building model as presented in Fig. 2, and the LTDH network and the WH are not modelled. The electricity demand of the HP is directly determined by the deterministic HD and thus is implemented as a time series.

3.3. Input data

The representative scenarios for heat demand, electric demand, PV irradiation, ambient temperature and electricity price are based on historical data. The PV data was generated for the location of Jülich, Germany, from the year 2019 based on [44]. The values for heating and electric demand are taken from local measurement data at Forschungszentrum Jülich. The k-medoids are used for clustering, as it has been demonstrated to be an effective algorithm for aggregating time-series data in energy systems [45]. Therefore, a time-series aggregation [46] is employed, resulting in representative scenario days. The scenario days have a respective weight w_{d} according to the number of days assigned to the cluster. For the building case study, the data was clustered into six scenario days with a time step length of one hour. Conversely, due to the computational burden of the model for the LEC case study, the aggregated data for the LEC was clustered into four scenario days, with twelve time steps of a constant length of $\Delta\tau = 2\,\mathrm{h}$. The representative scenario days for the single building case study are depicted in Fig. A.1, and for the LEC case study in Fig. A.2. The weights of the representative days are listed in Table 1.

The SOC of the BESS and the building temperature at the initial and final time steps of each representative day were set to be the same, respectively, with the specific values being determined by the optimisation. This ensures that no energy is transferred between representative days. Both case studies further consider a time-varying and constant electricity tariff to assess the impact of the type of electricity price tariff on the BESS sizing. The time-varying tariff incentivises load shifting to off-peak periods that align with lower electricity prices, resulting in peak-shaving and economic savings for buildings with batteries [47]. Input parameter values for BESS, PV data input and average of the time-varying electricity tariff are listed in Table 2, with the latter being used as the price for the constant electricity tariff. The input parameters for the components of the respective buildings are listed in Table A.1, including the values for the thermal storage of each building. The buildings, constructed between 1960 and 2011, have different sizes and temperature requirements. Depending on the size and the

Table 2
Key input parameters.

Component	Description	Parameter	Value
PV	High irradiance year	capacity factor	14.7%
PV	Medium irradiance year	capacity factor	14.0%
PV	Low irradiance year	capacity factor	13.8%
BESS	charging efficiency	η_{bess}^{in}	95 %
BESS	discharging efficiency	η_{bess}^{out}	95%
BESS	self-discharge rate	τ_{bess}	0.5 %/h
Grid	Time-varying tariff	average price	29.78 ct/kWh
Grid	feed-in tariff	revenue	5 ct/kWh

material of the building, their thermal capacity ranges from 100 kWh/°C to 600 kWh/°C. Furthermore, they can be categorised into two groups with respective input temperatures of 85 °C and 70 °C, representing the temperature requirement of the building for an ambient temperature of −12 °C. This input temperature is implemented as the condenser output temperature of the HP.

The GWI data for the external power grid and the BESS are sourced from licensed data from the ecoinvent database 3.9.1 as done in [48]. Specifically, the GWI data for the BESS is based on the market for a rechargeable, prismatic LiMn2O4 lithium-ion battery [49]. The optimisations are performed on a 1.8 GHz Intel Core i7-1265U CPU with 32 GB of RAM using Gurobi 10.0.1 [50] allowing non-convex quadratic constraints.

4. Results and discussion

In this section, the sizing of a retrofitted BESS within a multi-energy system is assessed. In Section 4.1, the results for a single building are presented, followed by designing a community BESS within a LEC in Section 4.2. For both case studies, the impact of time-varying and constant electricity prices on the BESS design is further assessed. Section 4.3 discusses the presented results.

4.1. Single building

For the single building case study, the BESS sizing results for the multi-energy and the *all-electric* modelling approaches are listed in Table 3. For a time-varying electricity tariff, the BESS capacity for the *all-electric* building is significantly bigger with an optimal size of 54.1 kWh compared to the multi-energy building with an optimal size of 14.4 kWh. For a constant electricity tariff, the BESS capacity for the *all-electric* building model and teh multi-energy model are within a similar range. The main reason for the smaller BESS size, especially for the time-varying tariff, is the considered TES which is coupled to the electricity system via the HP. The thermal inertia of the building provides additional flexibility which partly replaces the electrical flexibility offered by the BESS, thus resulting in a smaller BESS capacity. Additionally, the total annualised cost for the multi-energy model is between 6.1% and 6.5% lower than for the *all-electric* building model. This shows that explicitly modelling the operational flexibility of the heat coupled to electricity leads to lower system annualised cost. It can be further noted that the total annualised cost for the constant electricity tariff are 1.1% to 1.6% higher than for the respective model with time-varying electricity prices. The inability to exploit the time-varying tariff and shift demand to low-price hours results in an increase in the overall system cost.

The operational schedules for the multi-energy building and the *all-electric* building for six scenario days are depicted in Fig. 4. Positive values correspond to consumption and negative values represent generation. The active power is depicted with the state of charge (SOC) of the BESS, and for the multi-energy building model, the heat is depicted together with the building temperature. In the top part of Fig. 4(a), it can be seen that the power consumption of the HP directly follows the

Table 3
Optimal BESS size, annualised design and operational cost for the multi-energy building model and the *all-electric* building model for the time-varying and the constant electricity price tariff, respectively.

Tariff	Building model	BESS size	TAC	GWI
Time-varying	Multi-energy	14.4 kWh	35.5 k€/a	65.8 t_{CO_2}/a
	All-electric	54.1 kWh	37.8 k€/a	65.6 t_{CO_2}/a
Constant	Multi-energy	9.3 kWh	35.9 k€/a	66.8 t_{CO_2}/a
	All-electric	10.0 kWh	38.4 k€/a	71.9 t_{CO_2}/a

heat demand, thus creating a deterministic HP load profile for the *all-electric* model in the middle part of the figure. The BESS is fully charged and discharged[1] once during each day, taking advantage of the price fluctuations during each scenario day and the electricity generation of the PV array. The BESS is usually charged during hours of low electricity prices or hours of solar irradiance, and discharged during hours of high electricity prices. Due to the fixed power factors of the HP and the ED, the reactive power demand is deterministic, which is compensated by the reactive power injection of the BESS and the PV array.

For the multi-energy building, a significant difference can be observed for the HP operation in the upper part of Fig. 4(b), as it does not follow the heat demand directly. Instead, the HP mainly operates during hours of low electricity prices and high solar irradiation, to meet the heat demand and further charge the TES as can be seen by an increasing building temperature. The HP thus makes use of the thermal inertia of the building by heating it prior to times of high electricity prices, and thus less heating during high-priced hours is required. The building is heated during hours of solar irradiance and its thermal storage is exploited during evening hours. This pattern can be especially observed during scenario days 174, 223 and 231, which represent warmer months of the year with low heat demand and high solar irradiation. Moreover, the HP mainly operates at full load as its efficiency increases with an increasing load utilisation. The BESS for the multi-energy building model is significantly smaller, but it has a similar operating pattern as the *all-electric* building model. Therefore, it can be concluded that the main reason for the large difference in BESS capacity between the multi-energy and *all-electric* building models is the lack of thermal flexibility for the latter one. By explicitly modelling the heating system and thus integrating the flexibility of the TES for the multi-energy building model, investing in additional electrical flexibility by a large BESS capacity is not required. Instead, the thermal domain provides a significant amount of flexibility which can be exploited by considering the interactions between electricity and heat with each other.

4.2. Local energy community

For the LEC, the same two modelling approaches were implemented, namely the multi-energy model and the *all-electric* model. The BESS size, the location of the BESS, and the total annualised cost are listed in Table 4.

Similarly to the building case study, the *all-electric* community BESS is oversized by 22.1% compared to the multi-energy model for the time-varying electricity tariff. For the constant electricity tariff, the BESS capacity for the*all-electric* model is oversized by 3.5% compared to the *all-electric* LEC model. The design results show that the considered heating sector interacting with the electricity sector significantly impacts the BESS design capacity. The additionally modelled TES enables a more flexible HP operation, directly impacting the electricity sector and the BESS sizing, which can be explained with operational results in Fig. 5 further below.

[1] Charging the BESS represents a power demand and thus positive active power values, whereas BESS discharging corresponds to an internal power generation and thus negative values.

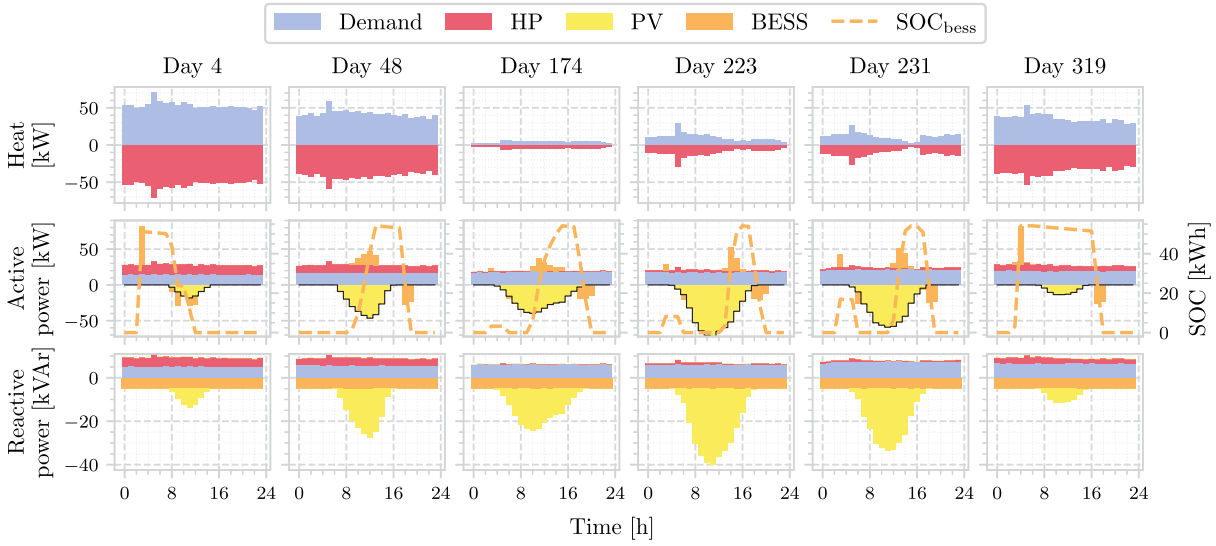

(a) *All-electric* building model

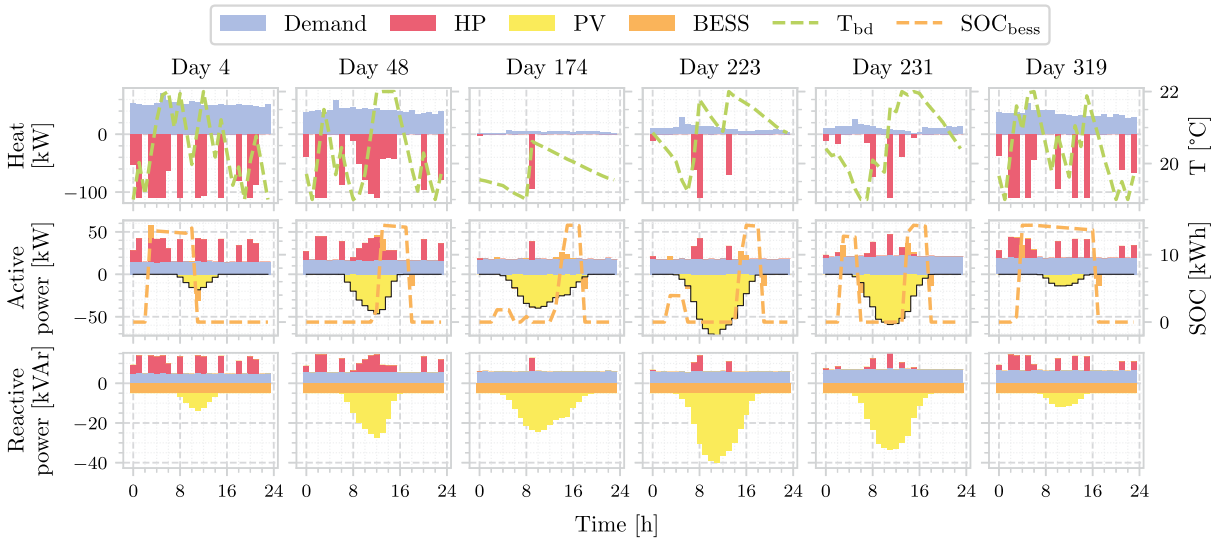

(b) Multi-energy building model

Fig. 4. Operational results of the heat, the active power and the reactive power for time-varying electricity tariff. Positive values represent demand and negative values represent generation.

Table 4
Optimal BESS size, location of the BESS, annualised design and operational cost for the multi-energy and the *all-electric* LEC models for the time-varying and the constant electricity price tariff, respectively.

Tariff	LEC model	Location	BESS size	TAC	GWI
Varying	Multi-energy	Bd 5	507 kWh	308.4 k€/a	426.8 t_{CO_2}/a
	All-electric	Bd 5	619 kWh	333.8 k€/a	459.1 t_{CO_2}/a
Constant	Multi-energy	Bd 5	548 kWh	310.7 k€/a	419.2 t_{CO_2}/a
	All-electric	Bd 5	567 kWh	337.1 k€/a	460.7 t_{CO_2}/a

The location for the community BESS is always chosen to be in building 5 (Bd5), which seems to be the optimal location at the head of the feeder close to the point of common coupling (PCC). Moreover, the total annualised cost for the *all-electric* LEC model are between 8.2% and 8.5% higher than for the multi-energy model, despite neglecting the operational cost for the LTDH network in the *all-electric* model. Furthermore, the annual GWI of the LEC increases by 7.6%–10.1% when not explicitly modelling the heating sector and its coupling to the electricity sector.

The operational results for the multi-energy community are presented in Fig. 5 for time-varying and constant electricity tariffs. It can be seen that for both modelling approaches, the HPs are operated in a manner that utilises the thermal inertia of the buildings in a similar pattern. However, for scenario day 317 representing a winter day with high heat demand and low PV generation, the time-varying electricity tariff depicted in Fig. 5(a) incentivises the BESS to be charged in the morning due to its low electricity prices compared to the remaining hours of this day. If the LEC pays constant electricity prices as shown in Fig. 5(b), the BESS remains at its lower limit as the PV generation is smaller than the electricity demand and there is no price incentive.

The impact of the solar irradiance on the BESS sizing is depicted in Fig. 6, where the same input data was used except for the different solar irradiance levels. Lower solar irradiance results in smaller BESS capacities, while high solar irradiance leads to larger BESS capacities independent of the chosen model and electricity tariff. It can further be seen that the multi-energy system models result in lower BESS

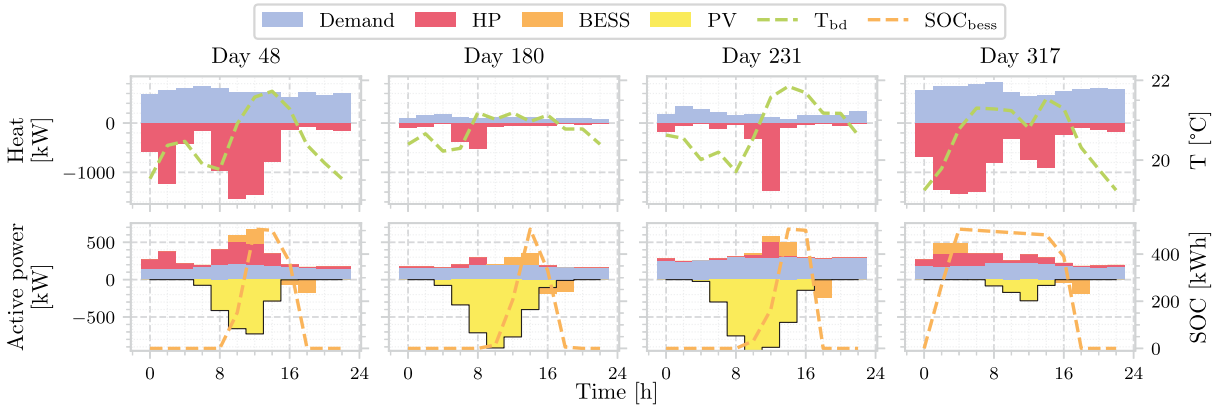

(a) Time-varying electricity tariff

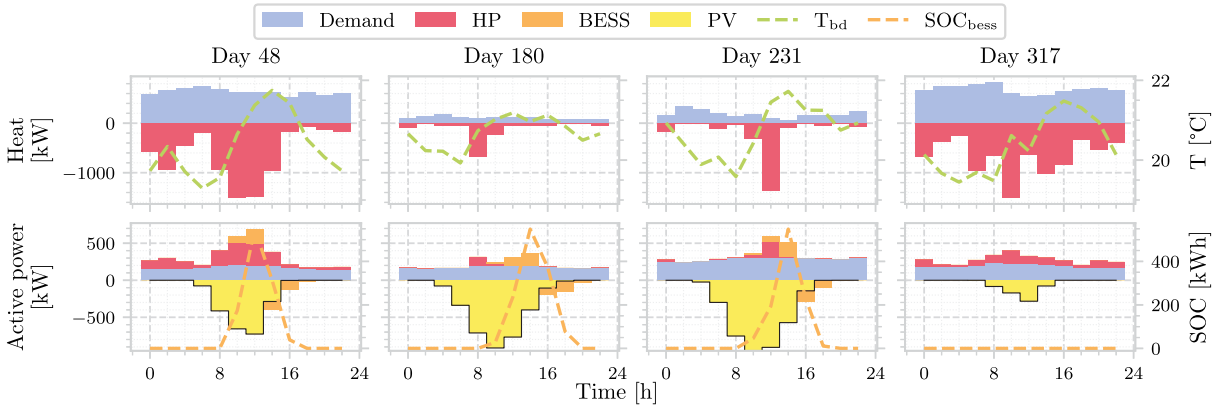

(b) Constant electricity tariff

Fig. 5. Operational results of heat and active power for the multi-energy LEC model. Positive values represent demand and negative values represent generation. Note that the values for demand, PV generation and building temperature are aggregated from all buildings within the LEC.

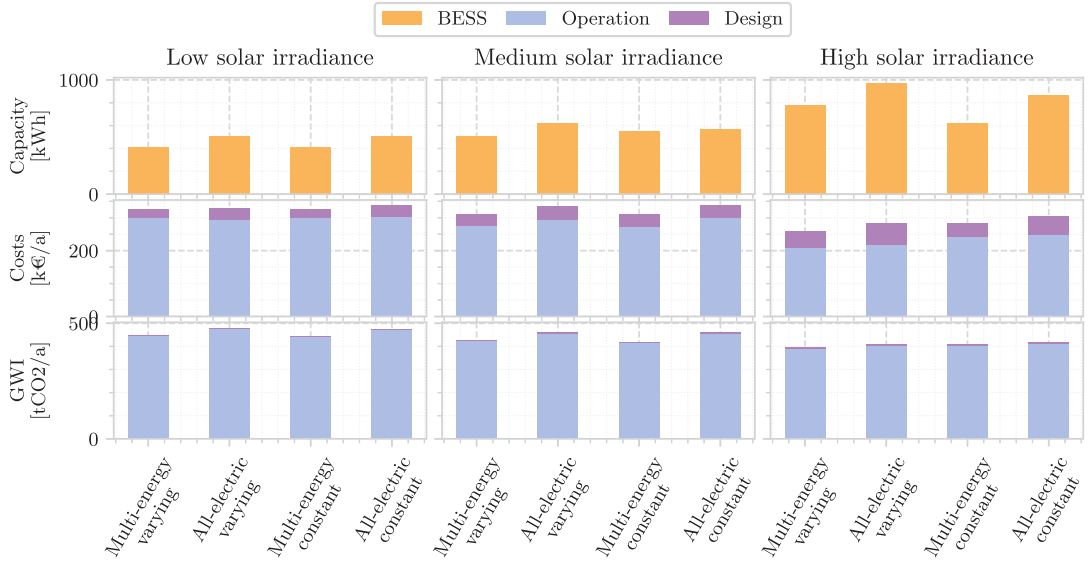

Fig. 6. BESS capacity (top), total annualised costs (middle) and annual global warming impact (GWI) (bottom) depending on the chosen model (multi-energy vs. *all-electric*) and electricity tariff (varying vs. constant) for the local energy community.

compared to their *all-electric* counterpart for the same tariff. Moreover, the impact of the annual GWI of the BESS is negligible compared to the annual GWI of the external power grid. However, the overall GWI decreases with larger BESS sizing as it can be seen for high solar irradiance, where the GWI and the annualised costs are the lowest.

Our results show that higher solar irradiance leads to a larger BESS capacity, reduced TAC and reduced annual GWI. Furthermore, a dynamic electricity tariff results in larger BESS sizes compared to a constant tariff for the all-electric system, which aligns with existing literature [51]. For an increasing solar irradiance, the BESS size difference between time-varying and constant tariff increases for the *all-electric* model. However, our findings indicate that when explicitly modelling the coupled thermal vector, the results vary depending on the solar irradiance. For low solar irradiance, the optimal BESS size is identical for both electricity tariffs. For medium solar irradiance, the time-varying tariff results in a 7.7% reduction of the BESS size, whereas for high solar irradiance, the optimal BESS size is by 25.9% larger than for the time-varying tariff.

4.3. Discussion

The results show that representing the heat vector solely from an electrical point of view and thus neglecting any operational flexibility of the coupled heating components alters the optimal design outcome of the BESS significantly. Taking into account the increasing electrification of the heating sector and for instance a future ban on fossil-fuel-based heating systems in Germany [52,53], the presented study is highly relevant as many households or LECs might consider retrofitting their systems with BESS. Our findings highlight the importance of explicitly modelling the thermal vector to avoid BESS oversizing. As shown in [54] for residential buildings, the thermal inertia of buildings allows the HPs to operate during hours of solar irradiance, thus increasing the PV self-consumption. Furthermore, our results indicate that the thermal flexibility of the building(s) also plays a pivotal role in the sizing of the retrofitted BESS capacity. The additional thermal flexibility decreases the need for electrical storage deployment, thus reducing investment and operational costs.

Including the heating demand for the *all-electric* models in the load profile of the heat pump without any operational flexibility leads to unfavourable or even unrealistic operating points. During hours of low heat demand, the heat pump directly follows the heat demand and thus operates at a very low part load, which is economically unfavourable due to the significantly lower coefficient of performance of the HP, increases the degradation and might not even be feasible in reality [55]. By explicitly modelling the heat commodity, including the part-load behaviour of the HP, these undesirable operating points can be effectively avoided. The thermal flexibility of the building was accounted for by the TES, which was modelled as a lumped parameter representing both the hot water storage and the thermal inertia of the building. It was combined with the deterministic heat demand based on historical data. Alternatively, if measurement data for the heat demand is unavailable, it could be replaced by an equivalent thermal resistance to represent the heat losses of the building. For the given model, the heat demand implicitly accounts for the heat losses. The temperature comfort level of each building was chosen to be between 19 °C and 22 °C. By increasing or decreasing this comfort level, the available thermal flexibility increases or decreases, respectively, which might further impact the BESS sizing. It is important to note that our findings only applies to energy systems with coupled electricity and heat commodities, which was the case for the given case study with the electric HP as the coupling component. If instead a classic gas boiler is as the heating technology, there would be no influence of the heating vector on the BESS size.

The presented work focuses on retrofitting an existing MES with a BESS. However, the underlying approach could be further applied to sizing an entire MES, for instance in the context of new building design. Considering the coupling between energy vectors could significantly influence the design of all components. For instance, the sizing of the HP might be impacted by the availability of stored energy in the BESS or the TES, potentially allowing for a smaller HP size. Additionally, the sizing and operation of the TES is highly correlated with the BESS, as an increase in one storage system could decrease the size of the other. By exploiting the storage systems of both commodities to store excess energy, the self-sufficiency of the MES can be increased as well. Furthermore, the size of the PV system might not only be influenced by the BESS but also indirectly by the heating sector. The electrical consumption of the heating sector affects the SOC of the BESS, thus impacting the capability to store access energy from the PV array. Therefore, an integrated design approach of electricity and heating components has the potential to reduce both design and operational costs while enhancing the self-sufficiency of the system.

Furthermore, there are various factors not considered that influence the BESS sizing and thus the generalisation of the presented findings. While the influence of different PV irradiation years on BESS sizing was demonstrated, the effect of different climate types could have a significant impact on the BESS size as well. Besides affecting solar irradiation, different climate types also directly impact energy consumption patterns. The colder the climate, the higher the heating demand, and thus potentially the bigger the impact of the coupled heating vector on the BESS sizing. Furthermore, the occupancy schedule and usage pattern can also influence the operational energy demand and thus the BESS sizing. Moreover, the specific characteristics of buildings such as insulation levels and construction materials affect overall thermal building inertia, further potentially influencing BESS sizing. Additionally, input data uncertainty, e.g., power demand, heat demand, price assumptions or PV irradiation, are potential limitations of the presented planning problem. The presented results and the identified findings are thus limited to the specific location and the assumed data.

While the GWI associated with the installation of BESS was considered in this study, it is important to acknowledge that other factors, such as disposal and recycling processes, also contribute to their overall environmental impact. Furthermore, for a greenfield design study, the GWI associated with other component installations such as PV array or HP must be taken into account as well. However, due to the scope limitations of our study, these additional aspects were not addressed in this analysis.

5. Conclusion

This study explores the impact of explicitly modelling the thermal vector on the optimal sizing of BESS within local multi-energy systems. A holistic problem formulation was developed, including the nonlinear representation of the AC power grid. On the one hand, the thermal vector was explicitly modelled with a quadratic model of the heat pump, the thermal inertia of the building and the heating network. On the other hand, the *all-electric* demand model implicitly included the electricity consumption of the thermal vector, thus neglecting any thermal flexibility. These two modelling approaches were applied to assess the impact of neglecting the thermal vector on the optimal BESS sizing in two real-world case studies: a single building and a local energy community. The results highlight the importance of integrated multi-energy modelling for retrofitting BESS, with several key findings:

- Rather than explicitly modelling the coupled heat vector, integrating the heat vector within an *all-electric* demand results in 9%–41% oversizing for a community BESS, and 176% for a building BESS with a time-varying tariff. The coupled thermal building flexibility reduces the need for the BESS to provide electrical flexibility.
- High solar irradiance increases BESS oversizing for *all-electric* demand models compared to integrated multi-energy models, and further increases the benefit of the time-varying electricity tariff compared to the constant tariff.

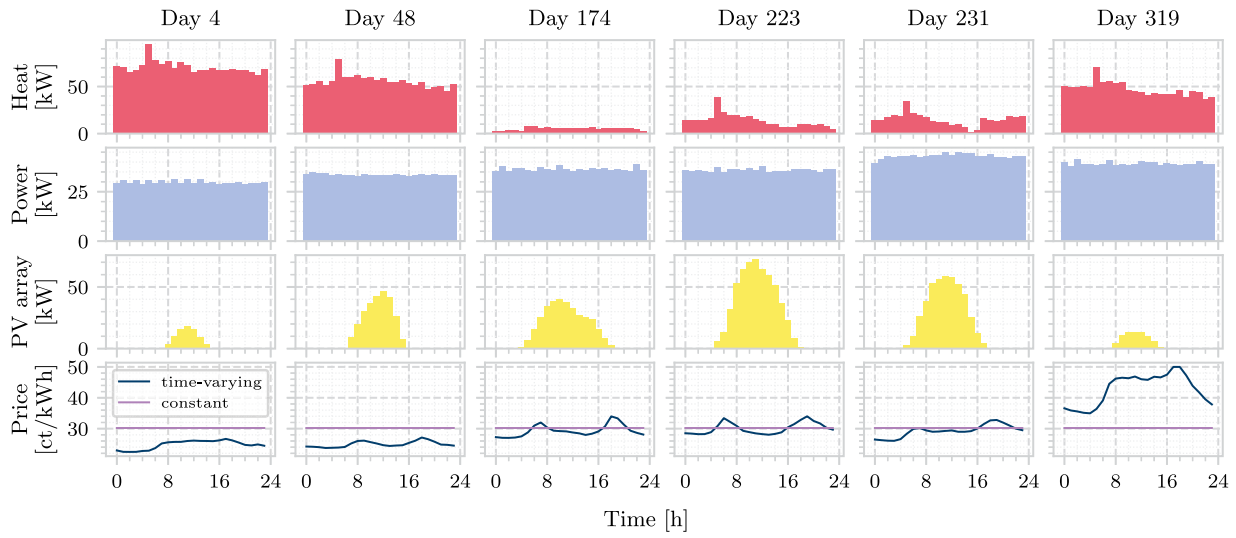

Fig. A.1. Clustered input data for the building case study with six representative cluster days.

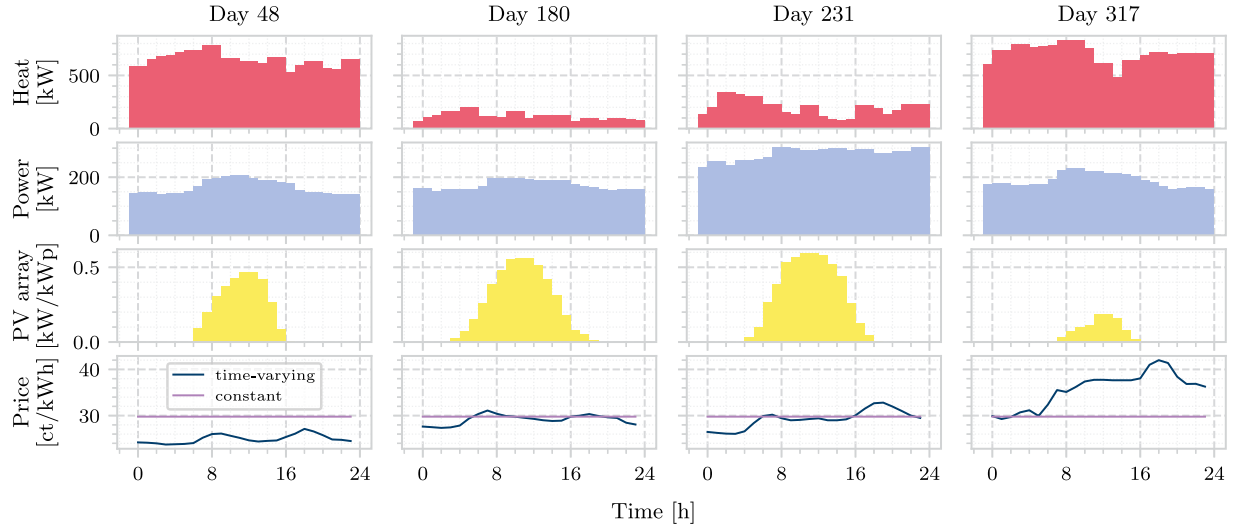

Fig. A.2. Clustered input data for the local energy community case study with four representative cluster days.

- Dynamic tariffs lead to larger BESS sizes for the *all-electric* system. Explicitly modelling the thermal vector introduces variability in BESS sizing, with differences between constant and time-varying tariffs across varying solar irradiance levels.
- The total annualised costs are reduced by up to 8.5% and the GWI by up to 8.3% when explicitly modelling the thermal vector, highlighting the economic and environmental benefits of integrated modelling of multi-energy systems.

Future research could investigate how other factors such as different climate types and user behaviour impact BESS sizing and expand the presented analysis to further components within multi-energy systems.

CRediT authorship contribution statement

Philipp Glücker: Writing – review & editing, Writing – original draft, Visualization, Software, Methodology, Investigation, Conceptualization. **Thiemo Pesch:** Writing – review & editing, Supervision, Funding acquisition. **Andrea Benigni:** Writing – review & editing, Supervision, Funding acquisition, Conceptualization.

Declaration of competing interest

The authors declare that they have no known competing financial interests or personal relationships that could have appeared to influence the work reported in this paper.

Data availability

The data that has been used is confidential.

Acknowledgements

We would like to thank Marco Langiu (RWTH Aachen University, Process Systems Engineering (AVT, SVT)) for providing valuable advice on the COMANDO framework, as well as Sonja Germscheid and Jan Stock (Forschungszentrum Jülich GmbH, Institute of Energy and Climate Research, Energy Systems Engineering (IEK-10)) for the insightful review of the manuscript. This work was funded by the Helmholtz Association of German Research Centres for programme-oriented funding through the Innovation Pool project "Energiewende und Kreislaufwirtschaft" (energy transition and circular economy).

Table A.1
Component parameters for the presented case study, which are chosen based on the real-world local energy community (LEC). The values of the heat demand and electric demand are based on historical measurement data of the LEC. Bd represents the respective building, whereas BB1 represents the upper bus bar to which the central PV array is connected.

Component	Symbol	Unit	Bd1	Bd2	Bd3	Bd4	Bd5	Bd6	Bd7	BB1
Building	K_{bd}	[kWh/°C]	300	100	600	100	100	600	200	–
Building	$T_{hp}^{con,max}$	[°C]	85	70	85	70	70	70	70	–
Heat pump	$\dot{Q}_{hp}^{max}$	[kW_{th}]	350	90	500	90	110	550	130	–
Heat	$\dot{Q}_{hd}^{max}$	[kW_{th}]	92.8	14.6	134.9	64.8	70.2	265.8	36.5	–
demand	$\dot{Q}_{hd}^{mean}$	[kW_{th}]	38.8	5.3	49.3	23.7	25.7	52.1	15.2	–
Electric	P_{ed}^{max}	[kW_{el}]	24.9	39.9	45.0	25.4	27.4	197.1	49.7	–
demand	P_{ed}^{mean}	[kW_{el}]	8.4	34.5	33.0	23.3	14.7	70.2	16.8	–
PV array	P_{pv}^{max}	[kWp]	80	80	80	100	80	150	80	1000

Appendix. Data input and parameters

Table A.1 presents the component parameters for the case study based on the real-world LEC. The values for the thermal building inertia K_{bd} stem from the dwellings and the hot water storage of the respective building.

Fig. A.1 depicts the six representative cluster days for the building case study. Fig. A.2 shows the four cluster days for the LEC case study. Note that the heat and power demand are aggregated over all buildings, and the active power generation from the PV array is normalised.

References

[1] Masson-Delmotte V, Zhai P, Pörtner H-O, Roberts D, Skea J, Shukla PR, Pirani A, Moufouma-Okia W, Péan C, Pidcock R, Connors S, Matthews J, Chen Y, Zhou X, Gomis MI, Lonnoy E, Maycock T, Tignor M, Waterfield T, editors. Global warming of 1.5° C: IPCC special report on impacts of global warming of 1.5° c above pre-industrial levels in context of strengthening response to climate change, sustainable development, and efforts to eradicate poverty. 1st ed.. Cambridge University Press; 2018, http://dx.doi.org/10.1017/9781009157940.

[2] European University Institute, Nouicer A, Kehoe A, Nysten J, Fouquet D, Meeus L, et al. The EU clean energy package. 2020 ed.. European University Institute; 2021, http://dx.doi.org/10.2870/58299.

[3] Weckesser T, Dominković DF, Blomgren EM, Schledorn A, Madsen H. Renewable energy communities: Optimal sizing and distribution grid impact of photovoltaics and battery storage. Appl Energy 2021;301:117408. http://dx.doi.org/10.1016/j.apenergy.2021.117408.

[4] Backe S, Zwickl-Bernhard S, Schwabeneder D, Auer H, Korpås M, Tomasgard A. Impact of energy communities on the European electricity and heating system decarbonization pathway: Comparing local and global flexibility responses. Appl Energy 2022;323:119470. http://dx.doi.org/10.1016/j.apenergy.2022.119470.

[5] Koirala BP, Koliou E, Friege J, Hakvoort RA, Herder PM. Energetic communities for community energy: A review of key issues and trends shaping integrated community energy systems. Renew Sustain Energy Rev 2016;56:722–44. http://dx.doi.org/10.1016/j.rser.2015.11.080.

[6] Li L, Cao X, Zhang S. Shared energy storage system for prosumers in a community: Investment decision, economic operation, and benefits allocation under a cost-effective way. J Energy Storage 2022;50:104710. http://dx.doi.org/10.1016/j.est.2022.104710.

[7] Dong S, Kremers E, Brucoli M, Rothman R, Brown S. Techno-enviro-economic assessment of household and community energy storage in the UK. Energy Convers Manage 2020;205:112330. http://dx.doi.org/10.1016/j.enconman.2019.112330.

[8] van der Stelt S, AlSkaif T, van Sark W. Techno-economic analysis of household and community energy storage for residential prosumers with smart appliances. Appl Energy 2018;209:266–76. http://dx.doi.org/10.1016/j.apenergy.2017.10.096.

[9] Walker A, Kwon S. Analysis on impact of shared energy storage in residential community: Individual versus shared energy storage. Appl Energy 2021;282:116172. http://dx.doi.org/10.1016/j.apenergy.2020.116172.

[10] Barbour E, Parra D, Awwad Z, González MC. Community energy storage: A smart choice for the smart grid? Appl Energy 2018;212:489–97. http://dx.doi.org/10.1016/j.apenergy.2017.12.056.

[11] Xiao J-W, Yang Y-B, Cui S, Liu X-K. A new energy storage sharing framework with regard to both storage capacity and power capacity. Appl Energy 2022;307:118171. http://dx.doi.org/10.1016/j.apenergy.2021.118171.

[12] Tao Y, Qiu J, Lai S, Zhao J. Integrated electricity and hydrogen energy sharing in coupled energy systems. IEEE Trans Smart Grid 2021;12(2):1149–62. http://dx.doi.org/10.1109/TSG.2020.3023716.

[13] Zhai J, Wu X, Zhu S, Yang B, Liu H. Optimization of integrated energy system considering photovoltaic uncertainty and multi-energy network. IEEE Access 2020;8:141558–68. http://dx.doi.org/10.1109/ACCESS.2020.3013396.

[14] Li N, Zhao X, Shi X, Pei Z, Mu H, Taghizadeh-Hesary F. Integrated energy systems with CCHP and hydrogen supply: A new outlet for curtailed wind power. Appl Energy 2021;303:117619. http://dx.doi.org/10.1016/j.apenergy.2021.117619.

[15] Koirala B, Hers S, Morales-España G, Özdemir Ö, Sijm J, Weeda M. Integrated electricity, hydrogen and methane system modelling framework: Application to the Dutch infrastructure outlook 2050. Appl Energy 2021;289:116713. http://dx.doi.org/10.1016/j.apenergy.2021.116713.

[16] Mallier L, Hétreux G, Thery-Hetreux R, Baudet P. A modelling framework for energy system planning: Application to CHP plants participating in the electricity market. Energy 2021. http://dx.doi.org/10.1016/j.energy.2020.118976.

[17] Mancarella P. MES (multi-energy systems): An overview of concepts and evaluation models. Energy 2014;65:1–17. http://dx.doi.org/10.1016/j.energy.2013.10.041.

[18] Mancarella P, Andersson G, Peças-Lopes J, Bell K. Modelling of integrated multi-energy systems: Drivers, requirements, and opportunities. In: 2016 power systems computation conference. 2016, p. 1–22. http://dx.doi.org/10.1109/PSCC.2016.7541031.

[19] Martínez Ceseña EA, Mancarella P. Energy systems integration in smart districts: Robust optimisation of multi-energy flows in integrated electricity, heat and gas networks. IEEE Trans Smart Grid 2019;10(1):1122–31. http://dx.doi.org/10.1109/TSG.2018.2828146, Conference Name: IEEE Transactions on Smart Grid.

[20] Martínez Ceseña EA, Loukarakis E, Good N, Mancarella P. Integrated electricity–heat–gas systems: Techno–economic modeling, optimization, and application to multienergy districts. Proc IEEE 2020;108(9):1392–410. http://dx.doi.org/10.1109/JPROC.2020.2989382, Conference Name: Proceedings of the IEEE.

[21] Liu X, Wu J, Jenkins N, Bagdanavicius A. Combined analysis of electricity and heat networks. Appl Energy 2016;162:1238–50. http://dx.doi.org/10.1016/j.apenergy.2015.01.102.

[22] Liu X, Yan Z, Wu J. Optimal coordinated operation of a multi-energy community considering interactions between energy storage and conversion devices. Appl Energy 2019;248:256–73. http://dx.doi.org/10.1016/j.apenergy.2019.04.106.

[23] Allegrini J, Orehounig K, Mavromatidis G, Ruesch F, Dorer V, Evins R. A review of modelling approaches and tools for the simulation of district-scale energy systems. Renew Sustain Energy Rev 2015;52:1391–404. http://dx.doi.org/10.1016/j.rser.2015.07.123.

[24] Capuder T, Mancarella P. Techno-economic and environmental modelling and optimization of flexible distributed multi-generation options. Energy 2014;71:516–33. http://dx.doi.org/10.1016/j.energy.2014.04.097.

[25] Gabrielli P, Gazzani M, Martelli E, Mazzotti M. A MILP model for the design of multi-energy systems with long-term energy storage. In: na AE, Graells M, Puigjaner L, editors. 27th European symposium on computer aided process engineering. Computer aided chemical engineering, vol. 40, Elsevier; 2017, p. 2437–42. http://dx.doi.org/10.1016/B978-0-444-63965-3.50408-6.

[26] Gabrielli P, Gazzani M, Martelli E, Mazzotti M. Optimal design of multi-energy systems with seasonal storage. Appl Energy 2018;219:408–24. http://dx.doi.org/10.1016/j.apenergy.2017.07.142.

[27] Bakken BH, Skjelbred HI, Wolfgang O. eTransport: Investment planning in energy supply systems with multiple energy carriers. Energy 2007;32(9):1676–89. http://dx.doi.org/10.1016/j.energy.2007.01.003.

[28] Clegg S, Mancarella P. Integrated electricity-heat-gas modelling and assessment, with applications to the great Britain system. Part II: Transmission network analysis and low carbon technology and resilience case studies. Energy 2019;184:191–203. http://dx.doi.org/10.1016/j.energy.2018.02.078, Shaping research in gas-, heat- and electric- energy infrastructures.

[29] Geidl M, Koeppel G, Favre-Perrod P, Klockl B, Andersson G, Frohlich K. Energy hubs for the future. IEEE Power Energy Mag 2007;5(1):24–30. http://dx.doi.org/10.1109/MPAE.2007.264850.

[30] Geng S, Vrakopoulou M, Hiskens IA. Optimal capacity design and operation of energy hub systems. Proc IEEE 2020;108(9):1475–95. http://dx.doi.org/10.1109/JPROC.2020.3009323.

[31] Morvaj B, Evins R, Carmeliet J. Optimising urban energy systems: Simultaneous system sizing, operation and district heating network layout. Energy 2016;116:619–36. http://dx.doi.org/10.1016/j.energy.2016.09.139.

[32] Liu X, Zhang P, Pimm A, Feng D, Zheng M. Optimal design and operation of PV-battery systems considering the interdependency of heat pumps. J Energy Storage 2019;23:526–36. http://dx.doi.org/10.1016/j.est.2019.04.026.

[33] Maroufmashat A, Sattari S, Roshandel R, Fowler M, Elkamel A. Multi-objective optimization for design and operation of distributed energy systems through the multi-energy hub network approach. Ind Eng Chem Res 2016;55(33):8950–66. http://dx.doi.org/10.1021/acs.iecr.6b01264.

[34] Piazza G, Delfino F, Bergero S, Di Somma M, Graditi G, Bracco S. Economic and environmental optimal design of a multi-vector energy hub feeding a local energy community. Appl Energy 2023;347:121259. http://dx.doi.org/10.1016/j.apenergy.2023.121259.

[35] Glücker P, Langiu M, Pesch T, Dahmen M, Benigni A. Incorporating AC power flow into the multi-energy system optimization framework COMANDO. In: 2022 open source modelling and simulation of energy systems. 2022, p. 1–6. http://dx.doi.org/10.1109/OSMSES54027.2022.9769138.

[36] Frank S, Rebennack S. An introduction to optimal power flow: Theory, formulation, and examples. IIE Trans 2016;48(12):1172–97. http://dx.doi.org/10.1080/0740817X.2016.1189626.
[37] Hering D, Cansev ME, Tamassia E, Xhonneux A, Müller D. Temperature control of a low-temperature district heating network with model predictive control and mixed-integer quadratically constrained programming. Energy 2021;224:120140. http://dx.doi.org/10.1016/j.energy.2021.120140.
[38] Bettanini E, Gastaldello A, Schibuola L. Simplified models to simulate part load performances of air conditioning equipments. In: Proc. IBPSA 8th int. conf. building simulation '03. 2003, p. 107–14.
[39] Waddicor DA, Fuentes E, Azar M, Salom J. Partial load efficiency degradation of a water-to-water heat pump under fixed set-point control. Appl Therm Eng 2016;106:275–85. http://dx.doi.org/10.1016/j.applthermaleng.2016.05.193.
[40] Sperber E, Frey U, Bertsch V. Reduced-order models for assessing demand response with heat pumps – insights from the German energy system. Energy Build 2020;223:110144. http://dx.doi.org/10.1016/j.enbuild.2020.110144.
[41] Romanchenko D, Kensby J, Odenberger M, Johnsson F. Thermal energy storage in district heating: Centralised storage vs. storage in thermal inertia of buildings. Energy Convers Manage 2018;162:26–38. http://dx.doi.org/10.1016/j.enconman.2018.01.068.
[42] Langiu M, Shu DY, Baader FJ, Hering D, Bau U, Xhonneux A, et al. COMANDO: A next-generation open-source framework for energy systems optimization. Comput Chem Eng 2021;152:107366. http://dx.doi.org/10.1016/j.compchemeng.2021.107366.
[43] Baumgärtner N, Delorme R, Hennen M, Bardow A. Design of low-carbon utility systems: Exploiting time-dependent grid emissions for climate-friendly demand-side management. Appl Energy 2019;247:755–65. http://dx.doi.org/10.1016/j.apenergy.2019.04.029.
[44] Pfenninger S, Staffell I. Long-term patterns of European PV output using 30 years of validated hourly reanalysis and satellite data. Energy 2016;114:1251–65. http://dx.doi.org/10.1016/j.energy.2016.08.060.
[45] Schütz T, Schraven MH, Fuchs M, Remmen P, Müller D. Comparison of clustering algorithms for the selection of typical demand days for energy system synthesis. Renew Energy 2018;129:570–82. http://dx.doi.org/10.1016/j.renene.2018.06.028.
[46] Domínguez-Muñoz F, Cejudo-López JM, Carrillo-Andrés A, Gallardo-Salazar M. Selection of typical demand days for CHP optimization. Energy Build 2011;43(11):3036–43. http://dx.doi.org/10.1016/j.enbuild.2011.07.024.
[47] Sepúlveda-Mora SB, Hegedus S. Making the case for time-of-use electric rates to boost the value of battery storage in commercial buildings with grid connected PV systems. Energy 2021;218:119447. http://dx.doi.org/10.1016/j.energy.2020.119447.
[48] Germscheid SHM, Nilges B, von der Assen N, Mitsos A, Dahmen M. Optimal design of a local renewable electricity supply system for power-intensive production processes with demand response. Comput Chem Eng 2024;185:108656. http://dx.doi.org/10.1016/j.compchemeng.2024.108656.
[49] Wernet G, Bauer C, Steubing B, Reinhard J, Moreno-Ruiz E, Weidema B. The ecoinvent database version 3 (part I): Overview and methodology. Int J Life Cycle Assess 2016;21(9):1218–30. http://dx.doi.org/10.1007/s11367-016-1087-8.
[50] Gurobi Optimization, LLC. Gurobi optimizer reference manual. 2023, https://www.gurobi.com. [Accessed on 01 Oct 2023].
[51] Mohamed AAR, Best RJ, Liu X, Morrow DJ. A comprehensive robust techno-economic analysis and sizing tool for the small-scale PV and BESS. IEEE Trans Energy Convers 2022;37(1):560–72. http://dx.doi.org/10.1109/TEC.2021.3107103.
[52] The Federal Government of Germany. New heating systems: using renewable energy sources as of 2024. In: Website of the federal government | bundesregierung. 2023, URL https://www.bundesregierung.de/breg-en/news/new-building-energy-act-2185010.
[53] Connolly K. Germany plans to ban installation of most oil and gas heating from 2024. Guardian 2023. URL https://www.theguardian.com/world/2023/apr/20/germany-plans-to-ban-installation-of-most-oil-and-gas-heating-from-2024.
[54] Rinaldi A, Soini MC, Streicher K, Patel MK, Parra D. Decarbonising heat with optimal PV and storage investments: A detailed sector coupling modelling framework with flexible heat pump operation. Appl Energy 2021;282:116110. http://dx.doi.org/10.1016/j.apenergy.2020.116110.
[55] García-Céspedes J, Arnó G, Herms I, de Felipe J. Characterisation of efficiency losses in ground source heat pump systems equipped with a double parallel stage: A case study. Renew Energy 2020;147:2761–73. http://dx.doi.org/10.1016/j.renene.2019.01.029, Shallow Geothermal Energy Systems.